On the Relative Intensities of Sea and Land Breezes

MAN KIN MAK AND JOHN E. WALSH

Laboratory for Atmospheric Research, University of Illinois, Urbana 61801

(Manuscript received 4 August 1975, in revised form 29 October 1975)

ABSTRACT

It is postulated that the observed difference in the intensities of sea and land breezes arises primarily from the diurnal variation of the stratification and the related variation of the eddy diffusion coefficients. Such time-varying properties of the medium are expected to give rise to a temporally asymmetrical circulation even when the surface forcing is symmetrical. This hypothesis is tested with a very basic sea breeze model that explicitly incorporates those physical processes mentioned above. The results demonstrate that the above hypothesis is valid. With the use of representative values for the parameters, the model yields a circulation that has a time-varying intensity and structure quite similar to those of observed sea and land breezes at different times of the day. The quantitative effects of the following important model parameters are also investigated: the relative phase angle between the forcing function and the stratification, and the magnitude as well as the vertical profile of the stratification and the eddy coefficients. Physical interpretations of those results are given.

1. Introduction

The diurnal cycle of onshore winds during the day and offshore winds at night is a characteristic weather feature in many coastal regions when the synoptic-scale pressure gradient is relatively weak. This wind regime is generally referred to as the sea and land breeze circulation. It is almost always observed, however, that the daytime sea breeze is stronger than the nighttime land breeze. An example is shown in Fig. 1, which is a time-height section of the observed wind component perpendicular to the coast above Santa Monica, Calif. The isopleths of wind speed, averaged over 29 sea breeze days, show that the daytime onshore flow is stronger than the nighttime offshore flow by a factor of about 3:2. Similar analyses of wind data from other locations would show that the ratio is often even higher. Significantly, such differences in wind speed are observed when the amplitude of the land-sea temperature contrast is as large at night as it is during the day. And, since the intensity differences are quite apparent when the synoptic-scale winds are negligible, they generally cannot be attributed to a prevailing gradient wind.

The differences between the land and sea breezes have received suprisingly little attention in the literature. Theoretical sea breeze studies generally fall into two categories. The first group consists of the analytic studies based on models which are of necessity quite simple and usually linear (e.g., Walsh, 1974; Smith, 1955; Defant, 1951). Since a sinusoidal time dependence (period = 24 h) is generally assumed, the land breeze is merely a mirror image of the sea breeze. The fact that the two phases are equal in intensity is one of the serious shortcomings of the linear treatments.

The second category of theoretical studies consists of the nonlinear numerical models, (e.g., Estoque, 1961; McPherson, 1970; Neumann and Mahrer, 1971; Pielke, 1974). While these models are more sophisticated, computational instability problems and cost limitations have generally prevented numerical simulations of periods longer than about 12 h. As a result, the daytime sea breeze has received considerable attention while the nighttime land breeze has again been largely ignored. An exception is the work of Neumann and Mahrer (1971), whose numerical computations produced a sea breeze which was stronger than the land breeze. An examination of Neumann and Mahrer's Eq. (15c), however, shows that their forcing function is asymmetric about the zero value. Specifically, their daytime land-sea temperature difference is about 2.5 times larger in magnitude than their nighttime value, as shown in Fig. 2. Since Neumann and Mahrer's exchange coefficients are functions of the Richardson number, their diffusivities may also be larger by day than by night. However, the imposition of an asymmetric surface temperature wave makes it impossible to isolate the effects of the forcing function from those of the stratification and/or the diffusivities.

This work will examine theoretically the differences between land and sea breezes in order to explain why the sea breeze is stronger than the land breeze in cases where the land-sea temperature contrast is equally strong during the two phases of the cycle. It should be noted that the observed daytime temperature contrast can be larger than, approximately equal to, or smaller

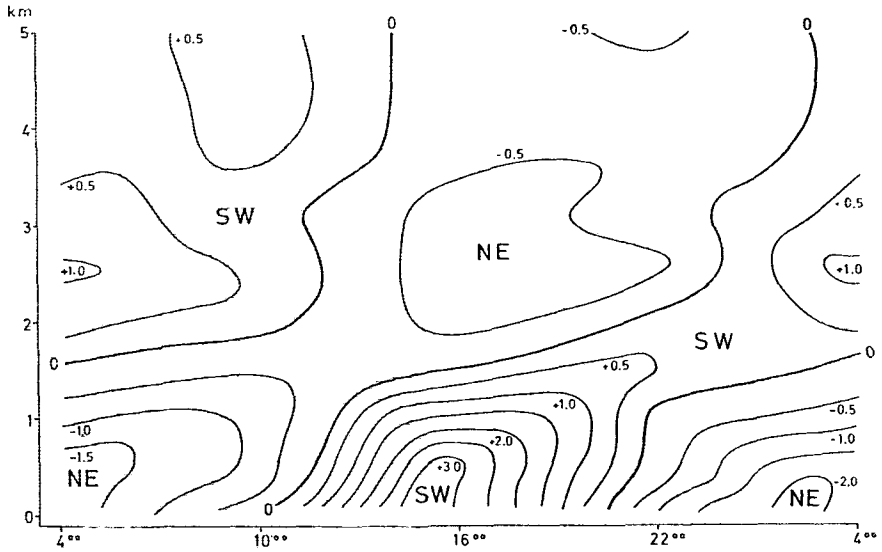

FIG. 1. The component of the wind perpendicular to the coast above Santa Monica, Calif., averaged over 29 sea breeze days. Positive values (m s^{-1}) indicate onshore winds. (From Flohn, 1969.)

than the nighttime contrast. Sea surface temperatures are primarily functions of the season, while daily averages of the soil temperatures vary with the season and with the synoptic weather situation. Daytime temperature contrasts are generally larger in the spring and early summer, while nighttime contrasts are usually larger in the late summer and autumn. Since the land breeze is almost invariably much weaker than the sea breeze, regardless of season, the asymmetry of the forcing function is evidently not the explanation. Rather, it is likely that the intensity differences stem from the fact that the static stability and the turbulent diffusivities of momentum and heat are functions of time, varying appreciably about their respective daily mean values. Such variations in the properties of the medium should give rise to an asymmetrical response over the course of one day even when the surface forcing is symmetrical. Mathematically speaking, the primary (symmetric) diurnal mode of the circulation is expected to interact with the diurnally varying properties of the medium, giving rise to higher harmonics and a time-independent mode. The higher harmonics in turn interact with the primary mode to generate still higher harmonics, and so on. Thus the response may be regarded as a superposition of a steady-state component and many other harmonics.

The theoretical model that will be used in this paper is a relatively simple one in which the static stabilities and eddy diffusivities are time- and height-dependent. In Section 2, the model is formulated and the method of solution is discussed. The results, which are presented in Section 3, include an examination of the role of the amplitudes of the stability and diffusivity variations.

2. Formulation of the model

The basic driving mechanism of the sea breeze phenomenon is the diurnal variation of the land-sea surface temperature contrast, which is conveniently introduced into this model as a lower boundary condition on the buoyancy $b=g(T-T_r)/T_0$, where g is gravity, $T_r(z)$ the base state temperature profile, and T_0 a reference temperature. We specify b at the surface $z=0$ as

$$b(x,0,t)=b_{\max}h(x)\sin\sigma t, \tag{1}$$

where σ is the diurnal frequency, $h(x)$ a function of x varying between $+1$ and -1, and $b_{\max}$ the amplitude of the surface buoyancy wave. The major physical features of interest are the time variations of the static stability and of the eddy coefficient. These are pre-

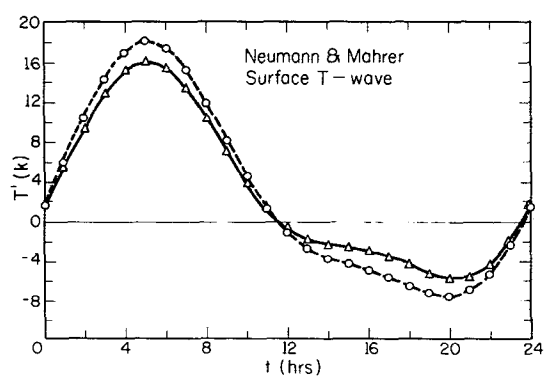

FIG. 2. Neumann and Mahrer's (1971) land-sea temperature differences computed using the land temperatures at 0 km (solid line) and 20 km (dashed line) from the coastline.

scribed respectively as

$$\frac{\partial \bar{b}}{\partial z} \equiv N^2 = N_0^2[1+\epsilon_1(z)\sin(\sigma t+\phi)], \tag{2}$$

$$K = K_0[1+\epsilon_2(z)\sin\sigma t], \tag{3}$$

where N_0^2 and K_0 are the daily mean values of N^2 and K, ϵ_1 and ϵ_2 the amplitudes of the daily fluctuations, and ϕ the relative phase with respect to the surface temperature. (The overbar denotes an average with respect to x, the coordinate axis perpendicular to the coastline.)

It should be noted that the two parameters ϵ_1 and ϵ_2 are used merely for generality in (2) and (3). Eddy diffusivities are known to be strongly dependent on the static stability, so it would clearly be unrealistic to assume that N^2 and K are independent functions. Indeed, this is why K and N^2 are linked to each other (and to the imposed surface temperature) by assuming the same functional form for the time-dependence. In the tests of Section 3, an additional physical constraint is imposed by assuming the same height-dependence in $\epsilon_1(z)$ and $\epsilon_2(z)$, i.e.,

$$(\epsilon_1,\epsilon_2) = (\epsilon_{1*},\epsilon_{2*})e^{-z/\lambda}, \tag{4}$$

where $0 \leqslant \epsilon_{1*} < 1$, $0 \leqslant \epsilon_{2*} < 1$. The relative magnitudes of the fluctuations in K and N^2, however, are somewhat uncertain, and it is for this reason that generality is retained through the use of two separate parameters ϵ_{1*} and ϵ_{2*}.

The special cases of $\epsilon_{1*} \neq 0$, $\epsilon_{2*} = 0$ and $\epsilon_{1*} = 0$, $\epsilon_{2*} \neq 0$ correspond to cases in which asymmetries are determined by stability fluctuations alone and by diffusivity variations alone. The interdependence noted above implies that these special cases bear less resemblance to physical reality than the cases in which both ϵ_{1*} and ϵ_{2*} are nonzero. The sensitivity tests described in Section 3 scan the possible values of ϵ_{1*} and ϵ_{2*}. The results of these tests will be examined with an eye toward the physical validity of the particular choices of ϵ_{1*} and ϵ_{2*}.

The choice of the vertical dependence in (4) also deserves mention. While our daily mean values (N_0^2 and K_0) of the stability and diffusivities are height-independent by (2) and (3), the fluctuations in N^2 and K are assumed to be largest near the surface by (4). The generally accepted profile of actual daytime eddy diffusivities, however, shows an increase from the surface up to a height of several tens to hundreds of meters. Above this height, most studies have assumed a somewhat arbitrary decrease in the value of K (e.g., Estogue, 1961; McPherson, 1970). The present treatment, with nonzero values of ϵ_{1*} and ϵ_{2*}, essentially neglects the daytime increase of K with height in the shallow surface layer. (The present model corresponds more closely to reality at night because the highest stabilities are then found at the surface.) The seriousness of the model's assumed K profile is addressed in Section 3, where the solution's sensitivity to λ is examined. It will be seen (Fig. 8) that the results are qualitatively the same whether $\lambda = 0$ (K = constant) or $\lambda \neq 0$ ($K \neq$ constant).

In order to simplify the analysis, we choose a simple periodic function for $h(x)$, namely one that consists of a sequence of step functions varying between $+1$ and -1 over a distance of L. Such a function is analytically represented as

$$h(x) = \frac{4}{\pi} \sum_{m=1,3,5\ldots} \frac{1}{n} \sin\frac{n\pi x}{L}. \tag{5}$$

This choice of $h(x)$ enables us to examine the response as a superposition of different Fourier harmonics in the x direction and should be an adequate representation of the sea-breeze phenomenon provided that L is sufficiently large. In the limit $L \to \infty$, (5) will approach a Fourier integral expansion.

Since we are primarily interested in testing the hypothesis that the diurnal variations of K and N^2 are responsible for the difference between the sea breeze and the land breeze, we deliberately neglect all other physical factors that are not essential to the occurrence of the sea breeze. Those factors include the coriolis effect, a mean flow, curvature in the coastline, and the horizontal diffusion of heat and momentum by small-scale eddies (Walsh, 1974). In the absence of the above processes and with the Boussinesq approximation, the governing equations may be written as

$$\left.\begin{aligned} u_t &= -p_x + Ku_{zz} \\ w_t &= -p_z + b + Kw_{zz} \\ b_t + N^2 w &= Kb_{zz} \\ u_x + w_z &= 0 \end{aligned}\right\}, \tag{6}$$

where p is the density-weighted departure of pressure from a reference pressure, and K and N^2 are given by (2) and (3). The thermodynamic equation in (6) is written in terms of the buoyancy b. It is the counterpart of the equation for a stratified incompressible fluid (Phillips, 1966) and is obtained by making use of the correspondence between density in the incompressible fluid and potential temperature θ in a stratified compressible fluid, together with the approximation $T'/T_0 = \theta'/\theta_0$, which is justified for a shallow system (θ_0 and T_0 are constant reference values).

The boundary conditions are

(i) $b(x,0,t) = b_{\max} h(x)\sin(\sigma t)$
(ii) $u(x,0,t) = w(x,0,t) = 0$
(iii) $\lim_{z\to\infty} u = \lim_{z\to\infty} w = \lim_{z\to\infty} b = \lim_{z\to\infty} p = 0$
(iv) cyclic x dependence of all variables (period $= L$).

The upper boundary conditions in (iii) do not include density factors because the Boussinesq assumption in (6) limits the validity of the system to the lowest several kilometers. In this region, $\rho u \to 0$ requires that $u \to 0$, for example.

The use of (5) for $h(x)$ suggests an expansion of the variables as follows:

$$\left.\begin{aligned}(w,b,p)&=\sum_{n=1,3,5,\ldots}\left(\sin\frac{n\pi x}{L}\right)(w_n,b_n,p_n)\\ u&=\sum_{n=1,3,5,\ldots}\left(\cos\frac{n\pi x}{L}\right)u_n\end{aligned}\right\}. \tag{7}$$

The following nondimensional quantities are then introduced:

$$\left.\begin{aligned}(\tilde{x},\tilde{z})&=\left(\frac{N_0}{K_0}\right)^{\frac{1}{2}}(x,z),\quad \tilde{t}=N_0 t,\quad \tilde{b}_n=\frac{b_n}{b_{\max}}\\ (\tilde{u}_n,\tilde{w}_n)&=\frac{N_0}{b_{\max}}(u_n,w_n),\quad \tilde{p}_n=\left(\frac{N_0}{K_0 b_{\max}{}^2}\right)^{\frac{1}{2}}p_n\\ \tilde{l}_n&=\frac{n\pi}{L}\left(\frac{K_0}{N_0}\right)^{\frac{1}{2}},\quad \tilde{\sigma}=\frac{\sigma}{N_0}.\end{aligned}\right\}.$$

The expansions (7) are substituted into (6) and the nondimensional quantities defined above are then introduced into the resulting equations. Upon dropping the tilde and the subscript n, we obtain for each n the following set of equations:

$$\left.\begin{aligned}&u_t=-lp+(1+\epsilon_2\sin\sigma t)u_{zz}\\ &w_t=-p_z+b+(1+\epsilon_2\sin\sigma t)w_{zz}\\ &b_t+[1+\epsilon_1\sin(\sigma t+\phi)]w=(1+\epsilon_2\sin\sigma t)b_{zz}\\ &-lu+w_z=0\end{aligned}\right\}. \tag{8}$$

It should be noted that the dependence on n is embodied in the parameter l.

The time-dependence of the variables is also represented spectrally by

$$q(z,t)=\sum_{m=-\infty}^{\infty}Q_m e^{im\sigma t},$$

where q may be u, w, b or p in (8). A set of governing equations for each m can then be obtained. Because of the time-dependent coefficients in (8), however, the Q_m are coupled to Q_{m-1} and Q_{m+1}. The equations for each m are

$$\left.\begin{aligned}&im\sigma U_m+lP_m-\frac{d^2U_m}{dz^2}=\frac{i\epsilon_2}{2}\frac{d^2}{dz^2}(U_{m+1}-U_{m-1})\\ &im\sigma W_m+\frac{dP_m}{dz}-B_m-\frac{d^2W_m}{dz^2}=\frac{i\epsilon_2}{2}\frac{d^2}{dz^2}\\ &\qquad\times(W_{m+1}-W_{m-1})\\ &im\sigma B_m-W_m-\frac{d^2B_m}{dz^2}=-\frac{i\epsilon_1}{2}(e^{i\phi}W_{m+1}\\ &\qquad-e^{-i\phi}W_{m-1})+\frac{i\epsilon_2}{2}\\ &\qquad\times\frac{d^2}{dz^2}(B_{m+1}-B_{m-1})\\ &lU_m-\frac{dW_m}{dz}=0\end{aligned}\right\}. \tag{9}$$

These equations are valid for $0\leqslant z\leqslant Z_T$ where Z_T is a sufficiently large value of z such that the solution does not appreciably depend on the particular value of Z_T. The boundary conditions for the spectral quantities are

$$\left.\begin{aligned}&U_m(0)=W_m(0)=0\\ &B_m(0)=-\frac{i}{2}\delta_{m,1}\\ &U_m(Z_T)=W_m(Z_T)=B_m(Z_T)=P_m(Z_T)=0\end{aligned}\right\}, \tag{10}$$

where $\delta_{m,1}$ is the Kronecker delta.

The presence of the coupling terms on the right side of (9) makes it impossible to write down the solution in analytic form. However, a rather simple numerical scheme may be used to determine Q_m for all m simultaneously. Centered differences are used to approximate d^2/dz^2 and d/dz in the first three equations in (9). However, it is necessary to use a forward difference expression for d/dz in the continuity equation in order to suppress the small but spurious oscillations that appear in the vertical structure of the solution when this derivative is represented by a centered difference. The resulting finite difference equations may be written in the matrix form

$$\begin{aligned}\mathbf{L}\mathbf{S}_m^{j-1}+\mathbf{M}\mathbf{S}_m^{j}+\mathbf{N}\mathbf{S}_m^{j+1}&=\mathbf{I}^j(\mathbf{S}_{m-1}^{j+1}+\mathbf{S}_{m-1}^{j-1}-\mathbf{S}_{m+1}^{j+1}-\mathbf{S}_{m+1}^{j-1})\\ &\quad+J^j\mathbf{S}_{m-1}^{j}+K^j\mathbf{S}_{m+1}^{j},\end{aligned} \tag{11}$$

for $j=1, 2, \ldots, j_{\max}$, $m=0, \pm1, \pm2, \ldots, \pm m_{\max}$. The superscript on each quantity indicates that this quantity is to be evaluated at the jth grid point. The height of the jth grid point is

$$z^j=\frac{(j-1)}{(j_{\max}-1)}Z_T\equiv(j-1)\Delta.$$

The vector $\mathbf{S}_m^j$ for each j and m is defined as

$$\mathbf{S}_m^j=\begin{bmatrix}U_m\\ W_m\\ B_m\\ P_m\end{bmatrix}_{z^j},$$

which has the boundary conditions

$$\mathbf{S}_m^1=\begin{bmatrix}0\\ 0\\ -\frac{1}{2}\delta_{m,1}\\ 0\end{bmatrix}\quad\text{and}\quad \mathbf{S}_m^{j_{\max}}=\begin{bmatrix}0\\ 0\\ 0\\ 0\end{bmatrix}.$$

The matrices $\mathbf{L}$, $\mathbf{M}$, $\mathbf{N}$, $\mathbf{I}^j$, $\mathbf{J}^j$ and $\mathbf{K}^j$ are:

$$\mathbf{L}=\frac{1}{\Delta^2}\begin{bmatrix}1&0&0&0\\ 0&1&0&0\\ 0&0&1&0\\ 0&0&0&0\end{bmatrix}$$

$$\mathbf{M}=\begin{bmatrix} -im\sigma-\frac{2}{\Delta^2} & 0 & 0 & -l \\ 0 & -im\sigma-\frac{2}{\Delta^2} & 1 & \frac{1}{\Delta} \\ 0 & -1 & -im\sigma-\frac{2}{\Delta^2} & 0 \\ l & -\frac{1}{\Delta} & 0 & 0 \end{bmatrix}$$

$$\mathbf{N}=\begin{bmatrix} \frac{1}{\Delta^2} & 0 & 0 & 0 \\ 0 & \frac{1}{\Delta^2} & 0 & -\frac{1}{\Delta} \\ 0 & 0 & \frac{1}{\Delta^2} & 0 \\ 0 & 0 & 0 & 0 \end{bmatrix}$$

$$\mathbf{I}^j=\frac{i}{2\Delta^2}\epsilon_2{}^j\mathbf{L}$$

$$\mathbf{J}^j=\begin{bmatrix} -\frac{i\epsilon_2{}^j}{\Delta^2} & 0 & 0 & 0 \\ 0 & -\frac{i\epsilon_2{}^j}{\Delta^2} & 0 & 0 \\ 0 & -\frac{i\epsilon_1{}^j}{\Delta^2}e^{i\phi} & -\frac{i\epsilon_2{}^j}{\Delta^2} & 0 \\ 0 & 0 & 0 & 0 \end{bmatrix}$$

and $\mathbf{K}^j$ is the complex conjugate of $\mathbf{J}^j$.

A particular maximum number of frequencies, $m_{\max}$, is appropriately chosen for each computational run, where $m_{\max}$ must be large enough that the results do not depend appreciably on that choice. It was found that $m_{\max}=6$ was adequate for small values of ϵ_{1*} and ϵ_{2*} and that $m_{\max}=12$ was needed when ϵ_{1*} and ϵ_{2*} exceeded 0.5. The physical basis for the spectral truncation is that the sufficiently high harmonics generated by the interaction between the primary component of the flow and the fluctuating parameters K and N^2 must be damped out by the viscous processes.

With a given value of $m_{\max}$, Eq. (11) is solved with the following iterative algorithm. The coupling terms on the right side of (11) are evaluated with the values of $\mathbf{S}_m^j$ obtained at the $(\nu-1)$th iteration in computing their values at the νth iteration. In this way, (11) may be treated as if it were a vectorial inhomogeneous algebraic equation for each m. The method of Lindzen and Kuo (1969) is used to solve for $\mathbf{S}_m^j$ from (11) at each iteration. To begin the iteration procedure, $\mathbf{S}_m^j$ is set to zero for all j and m. In most cases a high degree of convergence was achieved after only five or six iterations.

3. Results and discussion

a. General features

Fig. 3 shows the evolution of the u field at $x=0$ for a case in which the stability is independent of height and in which the eddy coefficient are independent of both height and time ($\epsilon_1=0.5$, $\epsilon_2=0.0$, $\lambda\to\infty$). The phase angle ϕ is 180°, implying that the stability is weak during the day and strong during the night. Since the plotted values are for the coastline, Fig. 3 is a theoretical counterpart of Fig. 1. The significant result in Fig. 3 is that the daytime sea breeze is computed or "predicted" to be stronger than the nighttime land breeze by nearly a factor of 2. When the velocities are dimensionalized by

$$\frac{b_{\max}}{N_0}\approx\frac{10^{-1}\text{ m s}^{-2}}{10^{-2}\text{ s}^{-1}}=10\text{ m s}^{-1},$$

the maximum wind speeds in Fig. 3 are approximately 4.5 m s^{-1} at about 1400 and 2.5 m s^{-1} at about 0200 (all times local). (The choice of $b_{\max}=0.10$ m s^{-2} corresponds to a maximum land-sea temperature difference of 6°C or 10.8°F.)

The x dependence of a representative solution is shown in Fig. 4 which consists of two instantaneous x-z cross sections of the u field, the first for 1500 and the second for 0300. In this case, the parameters are $\epsilon_{1*}=0.8$, $\epsilon_{2*}=0.5$, $\phi=180°$ and $\lambda=500$ m. Fig. 4 shows that the sea breeze is not only stronger at the coastline, but that its horizontal and vertical extents are larger than those of the land breeze. The relative horizontal extents are quite consistent with observational data on

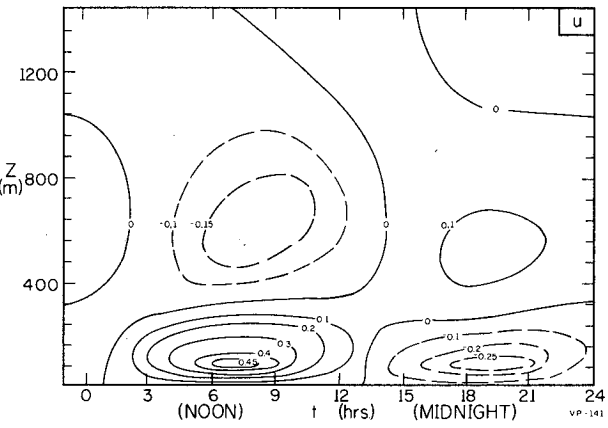

FIG. 3. The computed u component of the wind at $x=0$ for the case in which $\epsilon_1\equiv0.5$, $\epsilon_2\equiv0.01$, $\phi=180°$. Velocities and heights (both nondimensionalized) can be scaled by $N_0/b_{\max}=10$ m s^{-1} and $(K_0/N_0)^{\frac{1}{2}}=20$ m, respectively, as described in text.

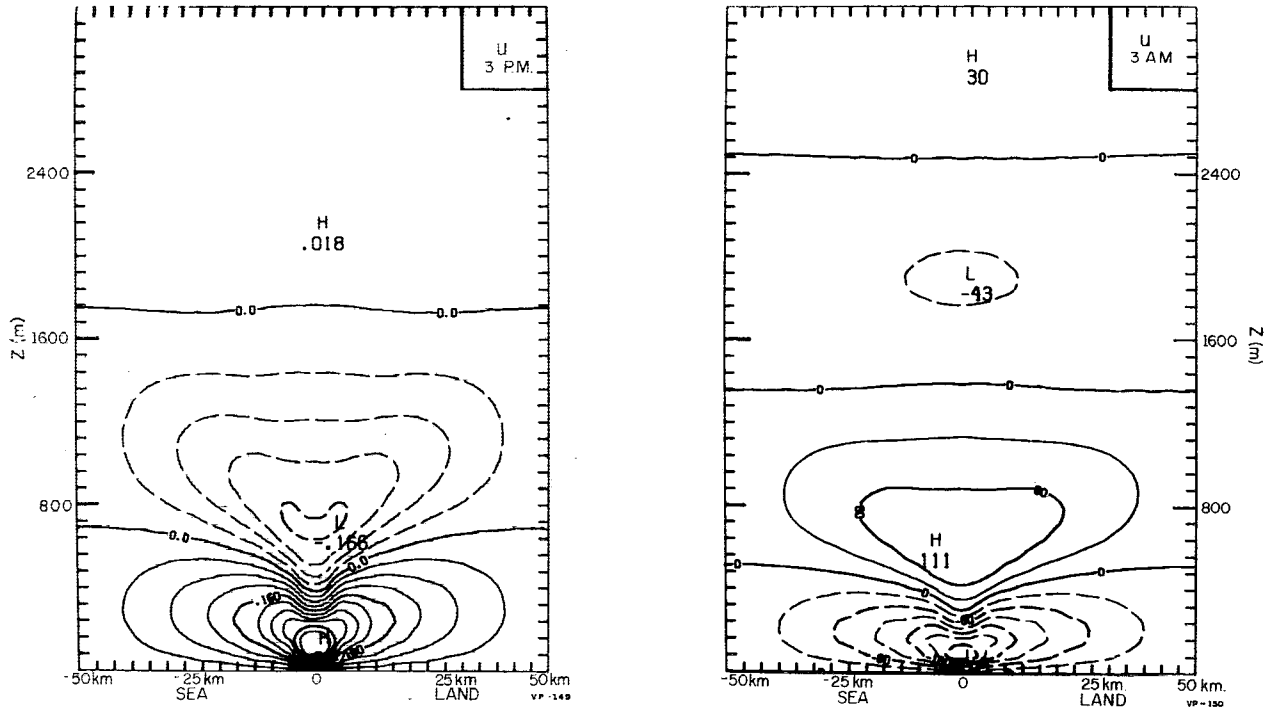

FIG. 4. The computed u component of the wind at 1500 and 0300 local time for the case in which $\epsilon_{1*}=0.8$, $\epsilon_{2*}=0.5$, $\lambda=500$ m, $\phi=180°$. Dimensionalization is described in text.

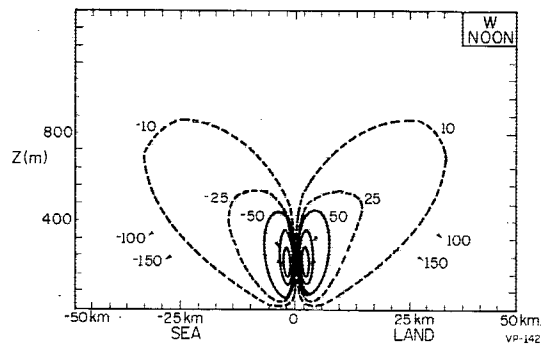

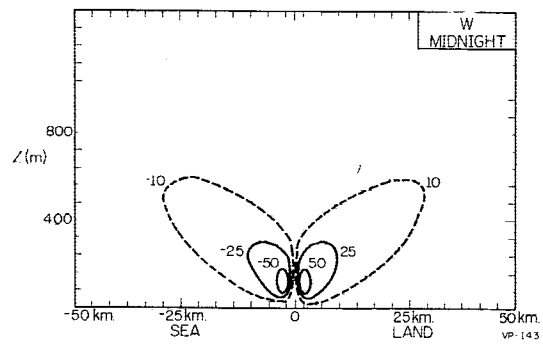

FIG. 5. The computed w component at 1200 and 2400 local time for the case in which $\epsilon_{1*}=0.8$, $\epsilon_{2*}=0.5$, $\lambda=500$ m, $\phi=180°$. Dimensionalization is described in text.

the sea breeze. The coordinates in the figure were dimensionalized by using

$$(K/N_0)^{\frac{1}{2}}=\left(\frac{4\ \mathrm{m^2\ s^{-1}}}{10^{-2}\ \mathrm{s^{-1}}}\right)^{\frac{1}{2}}=20\ \mathrm{m}.$$

It is also useful to examine the solution in terms of the vertical velocity field. Fig. 5 shows that the maximum value of w ($\sim$17 cm s^{-1} in dimensional form) is several times larger in the sea breeze than in the land breeze. The vertical motion also takes place through a considerably greater depth in the sea breeze phase of the cycle.

b. Sensitivity to ϵ_1 and ϵ_2

The sensitivity of the solution to the stability and diffusivity parameters was examined by scanning through the values of ϵ_{1*} and ϵ_{2*} in the range from 0 to 1. Fig. 6, based on computations in which centered differences were used for all derivatives, shows how the ratio of the maximum daytime u component to the maximum nighttime u depends on ϵ_{1*} and ϵ_{2*}. In these tests, ϕ is again 180° but a vertical dependence is now included in N^2 and the eddy coefficients with λ being equal to 500 m. In other words, the time-dependent parts of N^2 and K decay to e^{-1} of their surface values by a height of 500 m. As shown in the figure, the solution depends on ϵ_{1*} in the expected sense: the daytime/nighttime intensity ratio increases as the diurnal stability fluctuation becomes larger reaching a maximum

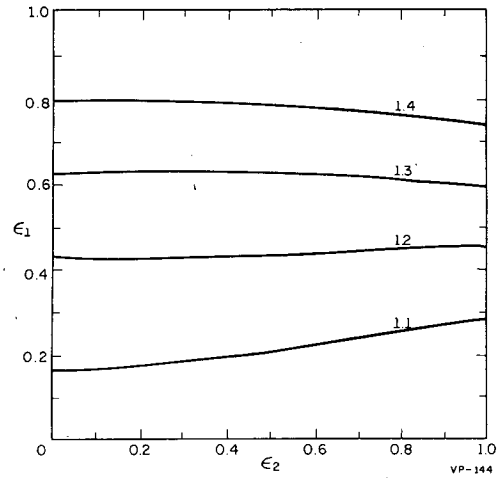

FIG. 6. The ratio $|u_{\max}|_{\text{day}}/|u_{\max}|_{\text{night}}$ as a function of the parameters ϵ_1 and ϵ_2.

value of about 1.5. However, the solution is quite insensitive to the parameter ϵ_{2*}. The apparent explanation here is that an increase in the diffusivity increases the eddy heat conduction (and therefore the driving for the circulation), but it also increases the viscosity. Since the driving and damping are both larger, the net result is little change in the intensity of the circulation.

Fig. 7 shows the ratio of the maximum daytime w component to the corresponding nighttime value. The dependence of this ratio on ϵ_{1*} is again considerably stronger than the dependence on ϵ_{2*}. It should be noted, however, that the dependence on ϵ_{2*} is more apparent than in the case of the u component. This result may be interpreted in terms of the differential dependence on ϵ_{2*} of the horizontal extent L and of the vertical extent D. To facilitate the discussion, we denote the maximum value of a quantity in daytime and

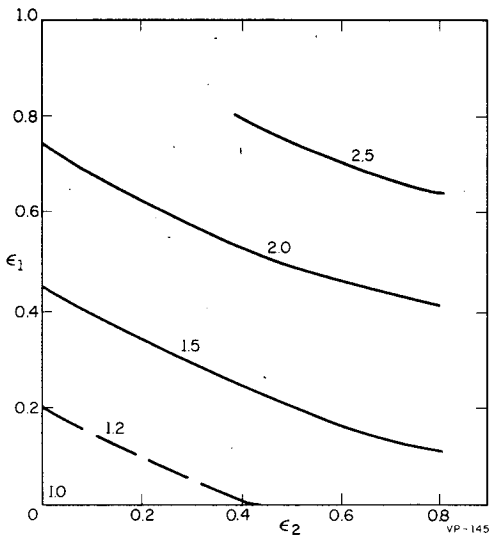

FIG. 7. The ratio $|w_{\max}|_{\text{day}}/|w_{\max}|_{\text{night}}$ as a function of the parameters ϵ_1 and ϵ_2.

nighttime by the subscripts d and n, respectively. From mass continuity considerations

$$\left|\frac{w_d}{w_n}\right| = \left|\frac{u_d}{u_n}\right| \frac{L_n}{L_d} \frac{D_d}{D_n}.$$

While the vertical extent is determined to a large extent by the magnitude of the diffusivity, the horizontal extent of the buoyancy contrast is largely controlled by the advection associated with the horizontal flow. Hence, as ϵ_{2*} is increased, D_d/D_n is expected to increase appreciably, much more so than L_d/L_n does. It follows that even though $|U_d|/|U_n|$ is practically independent of ϵ_{2*}, $|w_d|/|w_n|$ does increase noticeably with ϵ_{2*}.

As stated in Section 2, the fact that eddy diffusivities are strongly dependent on the vertical stability implies that ϵ_1 and ϵ_2 are not independent. It is for this reason that identical z and t dependences are specified for ϵ_1 and ϵ_2. For the same reason the cases in which ϵ_{1*} and ϵ_{2*} are both nonzero must be considered more physically realistic than the cases in which one and only one of $(\epsilon_{1*},\epsilon_{2*})$ is nonzero. Therefore, the most physically realistic portions of Figs. 6 and 7 are the upper right quadrants. One can say little more about the relation between ϵ_1 and ϵ_2 here except that the need to specify the two parameters independently is one of the model's shortcomings. It is quite possible that a more realistic model which formulates K in terms of the stability would give somewhat different results.

c. *Sensitivity to* λ

Since the choice of the vertical dependence of $\epsilon_1(z)$ and $\epsilon_2(z)$ is somewhat arbitrary, the sensitivity of the solution of the z dependence of ϵ_1 and ϵ_2 deserves attention. In the results of Figs. 4–7, both ϵ_1 and ϵ_2 have been of the form

$$(\epsilon_1,\epsilon_2) = (\epsilon_{1*},\epsilon_{2*})e^{-z/\lambda},$$

where $\lambda = 500$ m. Fig. 8 compares the u fields at $x=0$ for cases in which the damping height $\lambda = 500$ and 1000 m. Also shown are the results for $\lambda = 0$, or $\epsilon_1 = \epsilon_2 \equiv 0$. As the damping height increases, both the land breeze and sea breeze intensities peak at larger values, although the increase in the sea breeze intensity is somewhat larger. The sea breeze/land breeze intensity ratio increases from 1.37 for $\lambda = 500$ m to 1.68 for $\lambda = 1000$ m.

d. *Sensitivity to* ϕ

Fig. 9 shows the solution's sensitivity to the phase angle ϕ between the time of the stability maximum and local noon ($t=\pi/2$). (For $\phi = 180°$, the stability is weakest at noon; for $\phi = 90°$, it is weakest at sunrise.) It is apparent that the sea breeze/land breeze intensity ratio is largest when $\phi = 180°$. This result is reassuring because $\phi = 180°$ is probably the most reasonable phase angle to choose in view of the *observed* fact

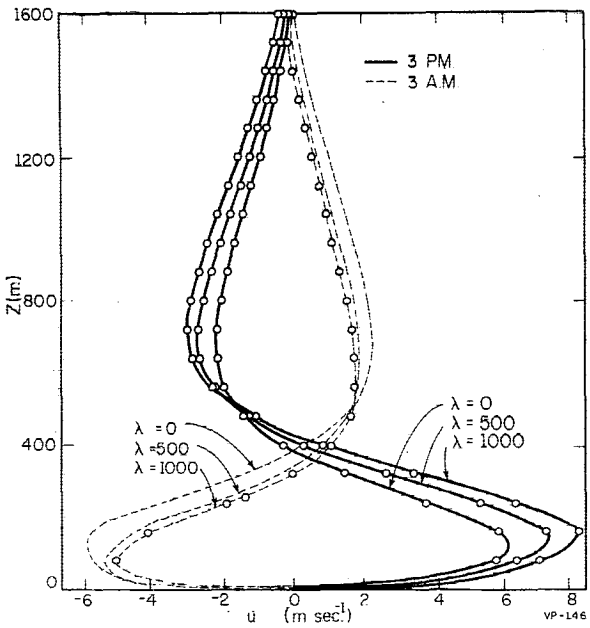

FIG. 8. The u component of the wind at $x=0$ for 1500 (solid lines) and 0300 (dashed lines). Results are shown for $\lambda=0$, 500 and 1000 m.

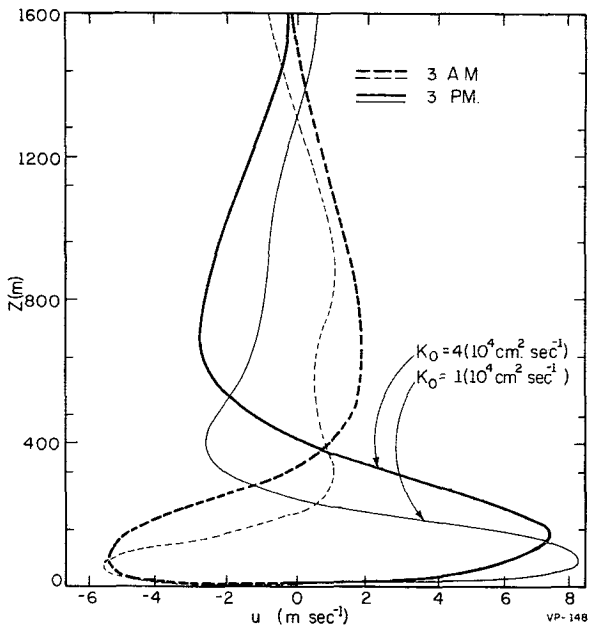

FIG. 10. The u component of the wind at $x=0$ for 1500 (solid lines) and 0300 (dashed lines). Results are shown for $K_0=10^4$ and 4×10^4 cm^2 s^{-1}.

that the atmosphere is generally the least stable within several hours of local noon. Fig. 9 also shows that the daytime and nighttime circulations are of approximately the same intensity when the stability maximum occurs at sunrise. This result is also intuitively reasonable, since both the daytime and nighttime 12 h periods have the same mean stability when $\phi=90°$. It is to be noted that the symmetry of the problem enables the results for the phase angle ϕ to be applied to $\phi+180°$ simply by switching day and night.

e. Miscellaneous results

Several additional cases were examined in order to determine the solution's sensitivity to the mean stability N_0 and the mean diffusivity K_0. Fig. 10 shows

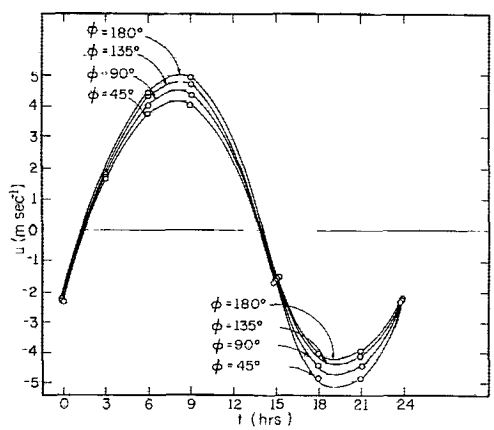

FIG. 9. The u component of the wind at $x=0$, $z=\Delta$ as a function of time for $\phi=0°$, 45°, 90°, 135°.

the effect of a reduction of the value of K_0 from 4 to 1 m^2 s^{-1} with $\epsilon_1=0.8e^{-z/\lambda}$, $\epsilon_2=0.5e^{-z/\lambda}$, $\lambda=500$ m. In the case of the smaller K_0, both the daytime and the nighttime circulations are considerably shallower. These results are consistent with the fact that the eddy conductivity distributes vertically the horizontal temperature contrast, which is the circulation's driving mechanism. The quantity

$$[\mathrm{KE}]_{x=0}=\frac{1}{2}\left[\int_{z=0}^{z_T}\rho u^2 dz\right]_{x=0},$$

which is the total kinetic energy of the circulation at the coastline, is noticeably smaller when K_0 is reduced. This result is to be expected because a smaller K_0 mixes less heat upward, resulting in a weaker horizontal pressure gradient at higher levels and therefore a considerably more rapid decrease in wind speed (and kinetic energy) with height. Near the surface, however, the maximum wind speeds in Fig. 10 do not appear to change significantly when K_0 is reduced, in agreement with the earlier statement that a smaller K implies less frictional damping. In short, the effect of the smaller K_0 is primarily felt at the upper levels due to a trapping of the differential solar heating near the surface.

The effect of increasing the mean static stability from 10^{-4} to 5×10^{-4} s^{-2} is shown in Fig. 11. The effect of a larger N_0^2 is to weaken the vertical motion, restricting the sea breeze circulation to a thinner layer. The circulation's horizontal extent is larger while its vertical extent is smaller. Similarly, the horizontal velocities at the coastline are larger while the vertical velocities are smaller. In other words, increasing the stability

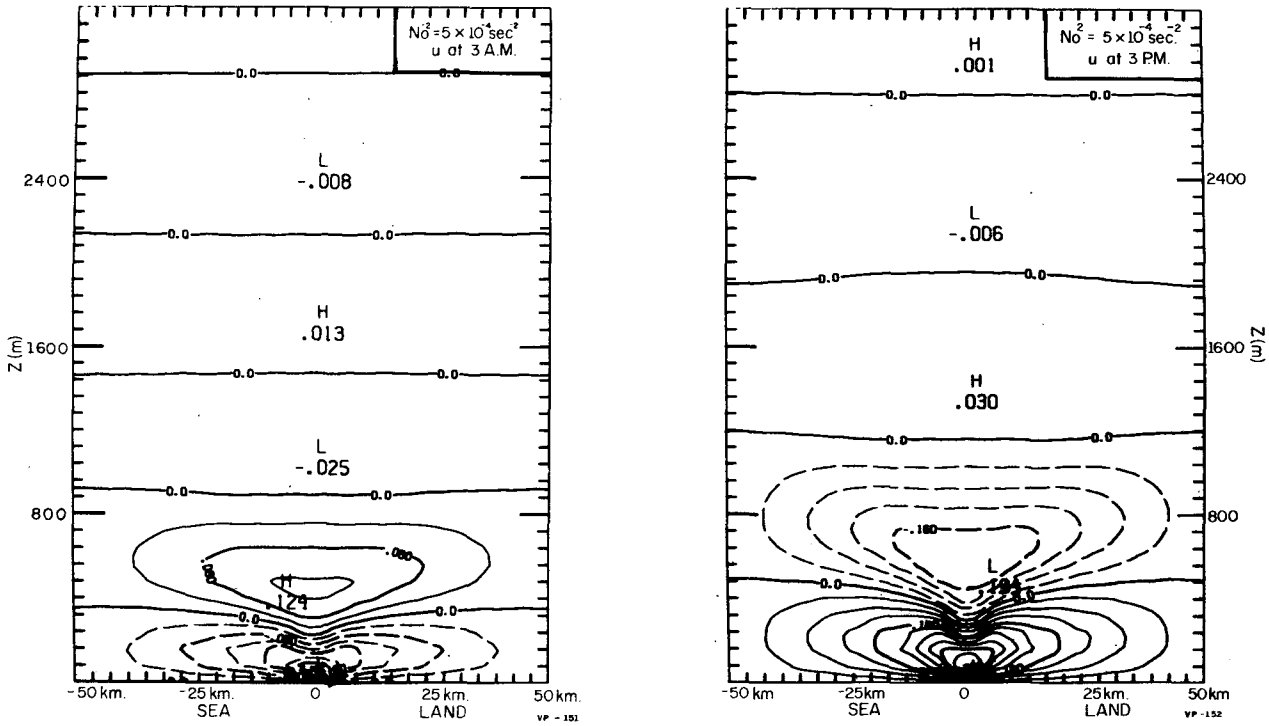

FIG. 11. As in Fig. 4 except for $N_0^2=5\times10^{-4}$ s^{-2}.

while keeping the eddy diffusivity constant tends to increase the horizontal kinetic energy and decrease the vertical kinetic energy.

4. Summary and conclusions

The results of Section 3 show that the major differences between land and sea breeze circulations can be attributed to the diurnal variations in the static stability and the eddy diffusivities. Even though the stability and diffusivity variations given by (2) and (3) are quite simple, their inclusion in a model produces a daytime sea breeze circulation which has stronger wind speeds and noticeably larger horizontal and vertical extents than the nighttime land breeze. Of the two effects, the stability fluctuations seem to play a more important role than the diffusivity variations. The lesser role of the latter is most likely due to the simultaneous increases in the conductive driving mechanism and in the viscous damping that result from an increase in the diffusivity.

The functional forms which were chosen for K and N^2 are indeed somewhat arbitrary. However, in view of the scarcity of measurements of the spatial and temporal variations of these parameters, the choices here seem as reasonable as any. Moreover, the primary aim of this work was to gain some qualitative physical insight into the differences between the land and sea breeze circulations. The fact that the results obtained here are quite compatible with the little data that do exist suggests that the choice of the vertical dependence of K and N^2 is not crucial.

As far as practical applications are concerned, it seems that the land breeze is still deserving of more attention. The occurrence of an onshore sea breeze flow during the day has obvious consequences on the atmospheric variables and the general air quality of many coastal population centers. It follows that the atmospheric state of the immediate coastal environment at night may depend quite strongly on the occurrence or non-occurrence of an offshore land breeze.

Acknowledgments. This research was supported by the Atmospheric Science Section, National Science Foundation, under Grants DES-7401188 and GA 40390. Part of the computations were done on the Control Data 7600 computer at the National Center for Atmospheric Research which is sponsored by the National Science Foundation. The authors wish to thank the several anonymous referees for their constructive comments.

REFERENCES

Defant, F., 1951: Local winds. *Compendium of Meteorology*, Boston, Amer. Meteor. Soc., 655–662.

Estoque, M. A., 1961: A theoretical investigation of the sea breeze. *Quart. J. Roy. Meteor. Soc.*, **87**, 136–146.

Flohn, H., 1969: Local wind systems. *World Survey of Climatology*, Vol. 2, H. Flohn, Ed., Amsterdam, Elsevier, 139–171.

Lindzen, R. S., and H.-L. Kuo, 1969: A reliable method for the numerical integration of a large class of ordinary and partial differential equations. *Mon. Wea. Rev.*, **97**, 732–734.

McPherson, R. D., 1970: A numerical study of the effect of a coastal irregularity on the sea breeze. *J. Appl. Meteor.*, **9**, 767–777.

Neumann, R. J., and B. A. Mahrer, 1971: A theoretical study of the land and sea breeze circulation. *J. Atmos. Sci.*, **28**, 532–542.

Phillips, O. M., 1966: *Dynamics of the Upper Ocean*. Cambridge University Press, 261 pp.

Pielke, R., 1974: A three-dimensional numerical model of the sea breeze over south Florida. *Mon. Wea. Rev.*, **102**, 115–139.

Smith, R. C., 1955: Air motion over a heated land mass. *Quart. J. Roy. Meteor. Soc.*, **81**, 382–395.

Walsh, J. E., 1974: Sea breeze theory and application. *J. Atmos. Sci.*, **31**, 2012–2026.